Supplement of

Pathway-specific responses of isoprene-derived secondary organic aerosol formation to anthropogenic emission reductions in a megacity in eastern China

Huilin Hu, et al.

Correspondence: Yue Zhao (yuezhao20@sjtu.edu.cn); Jingyi Li (Jingyili@nuist.edu.cn)

S1. Sample preparation and analysis of iSOA polyol tracers

For the analysis of iSOA polyols, the samples were prepared with following procedures. An aliquot of quartz filter of ~17.35 cm^2 were cut from each sample and then ultrasonically extracted three times with 15 mL of dichloromethane: methanol (2:1, v/v, GC grade and LC-MS grade, respectively, CNW Technologies GmbH) for 15 min each time. Prior to extraction, 200 μL ketopinic acid (2 ppm) was spiked onto the filter as an internal standard. The extracts derived each time were filtered with a PTFE hydrophobic syringe filter (0.45 μm pore size, Millipore), combined, and then concentrated to 500 μL by a rotary evaporator (RE52A, Shanghai Yarong Biochemical Instrument), which was then blown to dryness under a gentle nitrogen stream (99.99%, Shanghai Keju Chemical Co., LTD) and reconstituted in 420 μL of dichloromethane: methanol (2:1, v/v). Subsequently, 120 μL of the solution were taken and blown to dryness under N2, followed by derivatization with 150 μL of N, O-bis-(trimethylsilyl) trifluoroacetamide (BSTFA)/pyridine (2/1, v/v, Sigma-Aldrich) in an oven at 85 ℃ for 2 h.

iSOA polyol tracers were analyzed by a GC-MS, the details of (QP2020, Shimadzu) equipped with SH-5MS column (30 m × 0.25 mm I.D., 0.25 μm film thickness, J&W Scientific). The GC-MS was operated in the electron ionization (EI) mode and the trimethylsilyl derivatives were analyzed under selected ion monitoring (SIM) mode. The GC oven was initially held at 80℃ for 5 min, heated at 3℃ min^{-1} to 200℃, held for 2 min, then increased to 300℃ at 15℃ min^{-1}, and held at 300℃ for 15 min. Temperatures of the injector, the ion trap, and the interface were set to 275℃, 200℃, and 300℃, respectively.

S2. Sample preparation and analysis of iSOA OS tracers

An aliquot of quartz filter (~17.35 cm^2) was taken from each sample, followed by 30 min of ultrasonic extraction in 3 mL of methanol (LC-MS grade, CNW Technologies GmbH) for two times. The extracts were filtered and concentrated to 250 μL under a gentle nitrogen stream, which were subsequently mixed with ultrapure water of the same volume and centrifuged under 4 ℃.

The supernatants obtained by centrifugation were analyzed using an ultra-performance liquid chromatography quadrupole time-of-flight mass spectrometer equipped with an electrospray ionization (ESI) source (UPLC-ESI-QToFMS) (Xevo G2-XS QToFMS, Waters), which was operated in the full scan and negative ion modes. An ethylene-bridged hybrid C_{18} column (2.1 mm ×100 mm, 1.7 μm particle size, Waters) was employed to separate the analytes. The eluents consisting of water with 0.1% acetic acid (eluent A) and methanol (eluent B) were injected at a flow rate of 0.33 mL min^{-1}, following a gradient elution program: 99% A held for the initial 1.5 min; decreased to 46% over 6.5 min and to 5% over 3 min; then decreased to 1% over 1 min, held for 2 min; and finally returned to 99% over 0.5 min, held for 1.5 min to balance

the pump pressure and column. The detailed ESI conditions were described in our previous studies (Wang et al., 2021; Yang et al., 2023). Data were processed by MassLynx v4.2.

S3. Gas-phase fraction estimation of iSOA tracers

Previous studies have illustrated that iSOA polyol tracers are semi-volatile and water-soluble, which can partition into OM or dissolve into aerosol liquid water, while OS tracers are considered non-volatile (Yee et al., 2020; Nguyen et al., 2015). Herein, optimized chemical equilibrium partitioning model were used to estimate the gas-organic phase and gas-aqueous phase partitioning of iSOA polyol tracers (Wania et al., 2015).

The gas–particle partitioning equilibrium can be described by the absorptive gas/organic matter partitioning coefficient ($K_{p,i}$, $m^3\ g^{-1}$),

$$K_{p,i}=\frac{c_{p,i}}{c_{g,i}C_{OA}} \quad (1)$$

Where $c_{p,i}$ is the tracer concentration in the organic aerosol phase ($\mu g\ m^{-3}$), $c_{g,i}$ is the tracer concentration in the gas phase ($\mu g\ m^{-3}$), and C_{OA} is the concentration of organic matter ($\mu g\ m^{-3}$). The $K_{p,i}$ can be calculated from the saturation mass concentration (C_i^*, $\mu g\ m^{-3}$) of the tracer via eq 2 (Pankow and James, 1994).

$$K_{p,i}=\frac{1}{\delta_i C_i^*}=\frac{RT}{10^6\delta M_i p_{L,i}^o} \quad (2)$$

Where δ_i is the activity coefficient of the compound i in the particle phase taking a value of 1 in this study, M_i is its molecular weight ($g\ mol^{-1}$), $p_{L,i}^o$ is the saturation vapor pressure (atm) that was estimated using EVAPORATION model (O'meara et al., 2014), R is the ideal gas constant of $8.21\times10^{-5}\ m^3\ atm\ mol^{-1}\ K^{-1}$, and T is the temperature in Kelvin.

The gas-aqueous phase partitioning equilibrium is described by Henry's Law. The gas-aqueous phase distribution (f_H) was calculated by eq 3:

$$f_H=\frac{C_{aq}}{C_{gas}}=10^{-6}\cdot H^*\cdot R\cdot T\cdot LWC_{total} \quad (3)$$

Where the C_{aq} and C_{gas} are the aqueous-phase and gas-phase concentrations of the tracers ($\mu g\ m^{-3}$), respectively; H^* is the effective Henry's law constant ($M\ atm^{-1}$), estimated based on the Henry's law constants of 2-MTs ($3.38\times10^{10}\ M\ atm^{-1}$) and 2-MG ($5.25\times10^{8}\ M\ atm^{-1}$) in water at 298 K (Zhang et al., 2023), with the aerosol acidity effect for 2-MG and the temperature dependence for both 2-MTs and 2-MG being taken into account (The detailed formula and parameters have been described in (Zhang et al., 2023); LWC_{total} ($\mu g\ m^{-3}$ air) is the sum of LWC associated with inorganic aerosol (LWC_{inorg}, calculated by ISORROPIA-II) and hygroscopic OA (LWC_{org}) (Wania et al., 2015; Zhang et al., 2023). The LWC_{org} was estimated

by eq 4 (Wania et al., 2015), The LWC_{org} was estimated to be lower than 1 μg m^{-3}, while LWC_{inorg} are ranging from 1- 50 μg m^{-3}.

$$LWC_{org}=\rho_w V_{org}\kappa_{org}\frac{1-a_w}{a_w} \quad (4)$$

Where ρ_w is the density of water, V_{org} is the volume of OA (calculated by the mass concentration of OM divided by its density assuming to be 1.2 g cm^{-3})), a_w is the water activity, assuming the same value as RH, κ_{org} represents the hygroscopicity parameter for the organic mixture, estimated by oxygen to carbon ratio (O:C) of organic aerosol via eq 5 (Pye et al., 2017; Rasool et al., 2021).

$$\kappa_{org}=0.14\times O{:}C+0.03 \quad (5)$$

In this study, the average O:C value (~ 0.35) observed for OA in Shanghai (He et al., 2020; Huang et al., 2013; Liu et al., 2018) was used for the calculation.

The fraction in each phase can be calculated by eqs 6-8:

$$F_{gas}=\frac{1}{1+C_{om}/C^*+f_H} \quad (6)$$

$$F_{org}=\frac{C_{om}/C^*}{1+C_{om}/C^*+f_H} \quad (7)$$

$$F_{aq}=\frac{f_H}{1+C_{om}/C^*+f_H} \quad (8)$$

The particulate fraction of 2-MTs and 2-MG are defined as the summed fraction in organic and aqueous phases ($F_p=F_{org}+F_{aq}$).

S4. Estimation of the wet particle diameter

According to κ-Köhler theory, the wet diameter of particle matter (D_{RH}) is relative humidity-dependent (Brock et al., 2016), calculated by eq 9 ：

$$\frac{RH}{100}=\frac{D_{RH}^3-D_d^3}{D_{RH}^3-D_d^3(1-k)}\exp\left(\frac{4\sigma_s M_W}{RT\rho_w D_{RH}}\right) \quad (9)$$

where D_d is the dry particle diameter; σ_s is surface tension of the particles; ρ_w and M_W are the density and molecular weight of water; R is the ideal gas constant; and T is the temperature (in K). *k* is calculated as (Petters and Kreidenweis, 2007),

$$k=0.01+0.63f_{NH_4}+0.51f_{NO_3}+0.81f_{SO_4}+0.18f_{WSOC}$$

Where f_x is the mass proportion of inorganic ion x in $PM_{2.5}$. The contribution of water-soluble organic compounds (WSOC) is not considered as the f_{WSOC} is small during the sampling campaign.

Table S1. Concentrations of identified isoprene-derived SOA compound classes, $PM_{2.5}$ and its components, trace gases, aerosol liquid water content (LWC) and acidity (pH), as well as meteorological parameters in urban Shanghai

	Summer- 15 n=23		Winter-15 n=20		Summer-19 n=23		Winter-19 n=20		Summer-21 n=24		Winter-21 n=28		2015		2019		2021	
	mean	STD	mean	STD	mean	STD	mean	STD	mean	STD	mean	STD	mean	STD	mean	STD	mean	STD
2-MG-OS (ng m^{-3})	4.57	5.18	1.26	0.56	4.49	5.89	1.16	0.54	5.46	5.91	1.14	0.43	3.04	4.13	2.94	4.59	3.21	4.61
2-MT-OS (ng m^{-3})	35.80	48.97	0.46	0.19	29.20	49.50	0.37	0.18	14.34	20.99	0.28	0.16	19.42	39.71	15.79	38.67	7.02	16.02
2-MTs (ng m^{-3})	12.27	11.80	0.51	0.34	18.95	25.27	0.42	0.28	14.95	20.04	0.40	0.39	6.98	10.50	10.82	20.93	7.23	15.43
C_5-alkene triols (ng m^{-3})	49.42	63.18	0.87	0.69	36.91	60.91	0.48	0.25	22.45	42.56	0.28	0.25	27.57	52.42	20.91	48.74	10.69	30.91
2-MG (ng m^{-3})	2.02	1.85	1.02	0.48	2.35	2.22	0.74	0.41	2.21	1.93	0.30	0.28	1.57	1.48	1.65	1.85	1.20	1.63
iSOA (ng m^{-3})	100.26	123.12	3.78	2.11	88.70	135.43	2.9	1.07	59.40	90.08	2.42	1.07	55.55	101.65	51.03	109.30	29.72	68.02
Cl^- (μg m^{-3})	0.07	0.15	1.51	1.00	0.33	0.22	1.03	0.58	0.17	0.12	1.29	0.77	0.73	1.00	0.66	0.55	0.77	0.79
NO_3^- (μg m^{-3})	0.96	1.10	16.56	10.05	3.41	3.18	14.06	9.96	1.64	0.98	16.83	9.67	8.19	10.40	8.36	8.89	9.70	10.39
SO_4^{2-} (μg m^{-3})	7.42	3.06	11.14	5.13	4.15	2.00	9.23	5.3	3.29	1.80	5.39	3.11	9.14	4.51	6.52	4.62	4.40	2.76
NH_4^+ (μg m^{-3})	2.69	1.70	10.15	5.10	1.40	1.11	6.21	4.07	0.99	0.87	6.00	3.34	6.15	5.24	3.63	3.74	3.65	3.54
OM (μg m^{-3})	7.38	11.90	16.21	11.63	6.19	7.48	11.06	9.78	4.38	2.89	9.32	9.32	11.47	8.45	8.46	5.75	7.00	5.20
EC (μg m^{-3})	2.48	3.18	3.95	2.75	1.48	1.64	2.2	2.02	0.94	0.62	1.99	1.99	3.16	1.64	1.82	0.95	1.50	0.94
$PM_{2.5}$ (μg m^{-3})	30.82	13.54	91.05	47.51	21.98	11.07	55.89	29.89	18.55	8.87	48.24	27.36	58.73	45.13	37.75	27.59	34.27	25.48
LWC (μg m^{-3})	9.57	4.50	31.69	16.83	5.01	3.32	29.16	19.78	4.26	2.51	14.96	12.39	19.82	16.21	16.24	18.20	9.94	10.58
pH	3.00	0.33	3.45	0.16	2.39	0.34	3.59	0.32	1.97	0.91	2.98	0.65	3.17	0.35	2.99	0.69	2.52	0.92
NO_2 (ppb)	17.75	6.38	36.27	13.66	13.40	4.55	35.65	10.14	9.40	4.49	33.39	12.99	25.85	13.75	24.02	13.55	22.35	15.60
MDA8 O_3 (ppb)	70.16	36.40	34.59	7.59	53.45	23.82	27.08	9.49	52.89	23.81	33.87	11.42	51.96	38.90	45.74	24.91	47.28	22.71
O_x (ppb)	64.55	24.71	57.02	8.97	46.78	16.83	52.31	9.00	46.45	17.45	58.23	7.94	61.26	19.81	49.42	13.94	52.81	14.44
T (℃)	30.20	2.29	7.22	3.12	30.54	2.27	6.24	1.72	29.83	1.31	6.74	2.97	19.55	11.91	19.24	12.43	17.60	11.87
RH	0.71	0.09	0.70	0.10	0.72	0.07	0.72	0.14	78.46	6.75	60.93	12.82	0.71	0.09	0.72	0.11	69.18	13.58

isoprene (ppb)	0.194	0.143			0.248	0.085	0.027	0.011	0.189	0.116	0.023	0.011			0.151	0.127	0.096	0.112
$[2\text{-MG-OS/2-MT-OS}]_{total}$	0.79	0.65	4.69	1.03	0.85	0.58	5.76	1.32	1.09	0.70	8.62	3.07	2.54	2.13	3.19	2.67	5.09	4.42
$[2\text{-MG-OS/2-MT-OS}]_{particle}$	0.44	0.36	2.63	0.58	0.48	0.33	3.23	0.74	0.61	0.39	4.64	1.71	1.43	1.2	1.79	1.5	2.63	2.38
$[2\text{-MG/2-MTs}]_{particle}$	0.25	0.25	2.57	1.45	0.24	0.19	2.41	2.7	0.18	0.09	1.16	1.13	1.29	1.52	1.19	2.08	0.66	0.92
$[IEPOX\text{-/HMML/MAE-SOA}]_{particle}$	11.06	6.74	0.78	0.29	7.80	6.27	0.75	0.22	5.62	2.99	0.73	0.41	6.43	7.16	4.71	5.85	3.12	3.23
$[IEPOX\text{-/HMML/MAE-SOA}]_{total}$	2.63	1.93	0.39	0.15	1.55	2.15	0.33	0.11	0.90	0.81	0.29	0.17	1.59	1.80	0.98	1.67	0.57	0.63

Table S2. Matrix effect factors of 2-methylerythritol and 2-MG standards and mass concentrations (μg m^{-3}) of major components in eight $PM_{2.5}$ filter samples.

Date of sample	NO_3^-	SO_4^{2-}	NH_4^+	OM	EC	$PM_{2.5}$	2-MG		2-methylerythritol	
							EXP 1	EXP 2	EXP1	EXP2
2019/7/31	0.36	1.67	0.33	3.93	0.94	11.45	0.86(1.0)	0.91(10.0)	1.18(1.0)	1.28(10.0)
2019/1/23	25.15	8.89	9.38	20.53	3.33	89.14	0.57(1.0)	0.69(10.0)	1.38(1.0)	1.26(10.0)
2015/8/9	0.78	2.6	0.71	1.34	0.76	6.45	0.63(1.0)	0.76(10.0)	1.11(1.0)	1.21(10.0)
2016/1/14	28.75	19.74	19.66	23.21	5.07	158.17	0.59(1.0)	0.83(10.0)	1.14(1.0)	1.35(10.0)
2021/7/21	1.05	2.54	0.44	3.18	0.3	12.58	0.83(1.0)	0.83(10.0)	1.13(1.0)	1.29(10.0)
2022/1/15	27.13	7.21	8.74	17.35	2.61	75.83	0.91(1.0)	0.85(10.0)	1.36(1.0)	1.29(10.0)
Mean							**0.73±0.15**	**0.81±0.07**	**1.20±0.10**	**1.28±0.05**

The values in parentheses are the concentrations (ppm) of the standards added to the filter sample extracts. The bold numbers are the mean matrix effect ratios.

Table S3. Key parameters for simulating reactive uptake of IEPOX/HMML/MAE on aqueous aerosols in the Base Case and Case 1.

Parameters	IEPOX		HMML/MAE	
	Base Case	Case 1	Base Case	Case 1
H^* at 298 K (M atm^{-1})	3.0×10^{7}	2.7×10^{6} [a]	1.2×10^{5}	7.5×10^{6} [b]
k_{H_2O,H^+}($M^{-2}\cdot s^{-1}$)	9.0×10^{-4}		9.0×10^{-4}	
$k_{SO_4^{2-},H^+}$($M^{-2}\cdot s^{-1}$)	8.83×10^{-3}		2.0×10^{-4}	
k_{H_2O,HSO_4^-}($M^{-2}\cdot s^{-1}$)	1.31×10^{-5}		1.31×10^{-5}	
$k_{SO_4^{2-},HSO_4^-}$($M^{-2}\cdot s^{-1}$)	2.92×10^{-6}		2.92×10^{-6}	

[a](Pye et al., 2013); [b](Zhang et al., 2023)

Table S4. Values of the Henry's law constant and gas-phase and aqueous-phase reaction rate constants with OH radicals of 2-MTs and 2-MG used in the model (Case 1).

Parameters [a]	2-MTs	2-MG
H^* at 298 K (M atm^{-1})	3.38×10^{10}	5.25×10^{8}
$k_{OH,gas}$ (cm^3 $molecule^{-1}$ s^{-1})	3.66×10^{-11}	6.87×10^{-12}
$k_{OH,aq}$ (M^{-1} s^{-1})	1.14×10^{9}	$(0.97\text{-}1.41)\times10^{9}$

The parameters listed in the table are all referenced from the model parameters described in (Zhang et al., 2023). The $k_{OH,aq}$ for 2-MG is pH-dependent, with $k_{OH,aq}$ equal to 9.7×10^{8} M^{-1} s^{-1} at a pH of 2 and 1.41×10^{9} M^{-1} s^{-1} at a pH of 5.

Table S5. Simulated concentrations of OH radicals and ratios of (MVK+MACR)/isoprene during the observation period.

Parameters	OH (10^6 cm^{-3})	(MVK+MACR) /isoprene
Summer-2015	3.29	7.72
Summer-2019	2.85	5.07
Winter-2015	0.34	0.58
Winter-2019	0.31	0.45

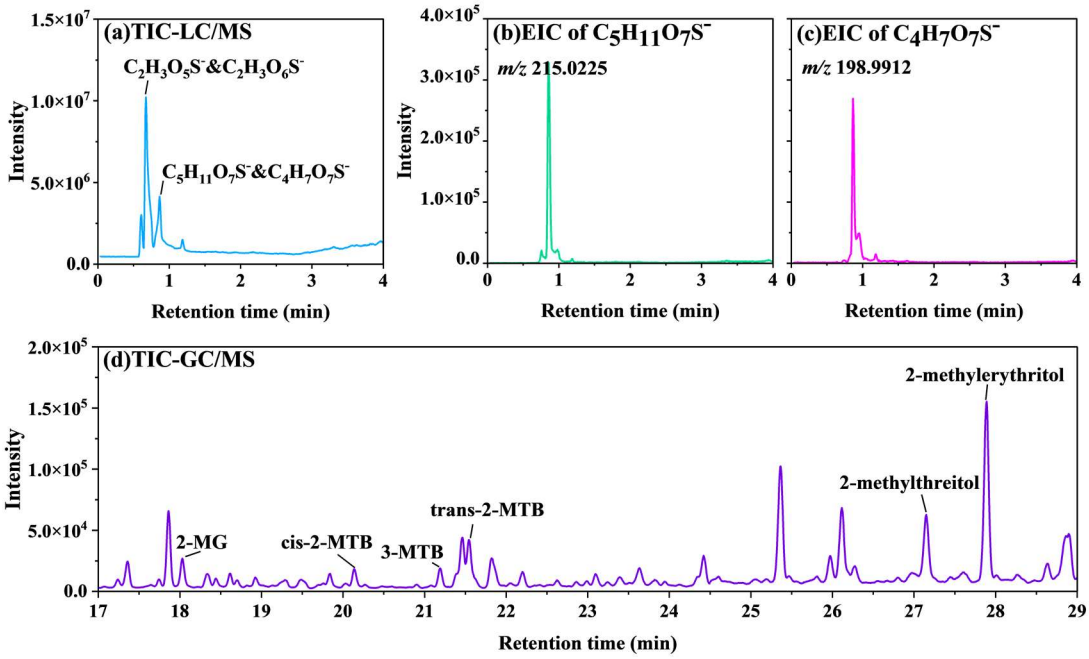

Figure S1. Example chromatograms of iSOA tracers in ambient PM2.5 samples. (a) Total ion chromatogram (TIC) of iSOA OSs from the LC-MS analysis; (b) and (c) Extracted ion chromatograms of 2-methyltetrol sulfate (2-MT-OS) and 2-methylglyceric acid sulfate (2-MG-OS), respectively; (d) TIC of a trimethylsilyl-derivatized iSOA polyol tracers from the GC-MS analysis.

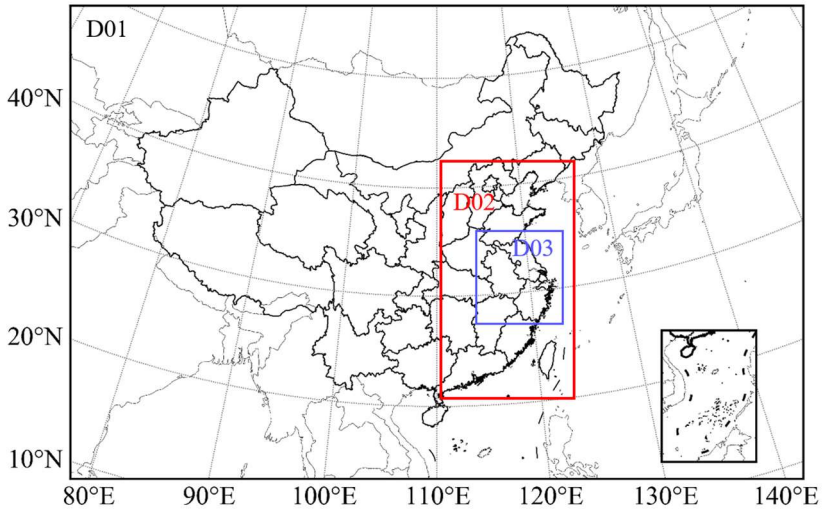

Figure S2. Three nested domains of CMAQ with horizontal resolutions of 36 km (D01), 12 km (D02), and 4 km (D03).

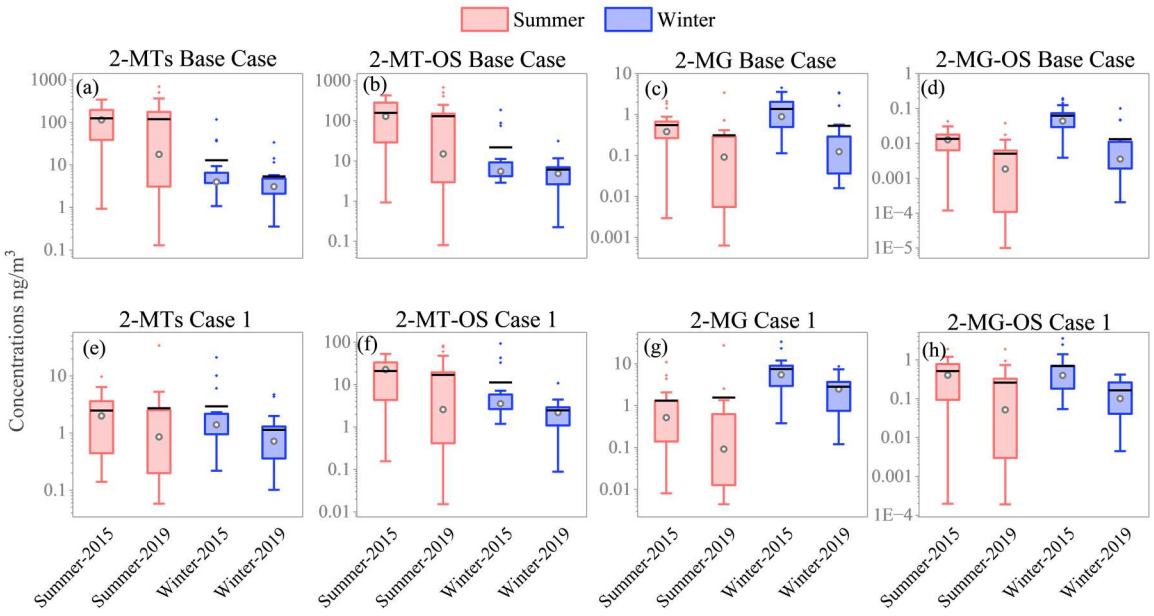

Figure S3. Simulations of iSOA tracers including 2-MTs, 2-MT-OS, 2-MG, and 2-MG-OS in Base Case (a, b, c, and d) and Case 1(e, f, g, and h) in summer and winter of 2015 and 2019.

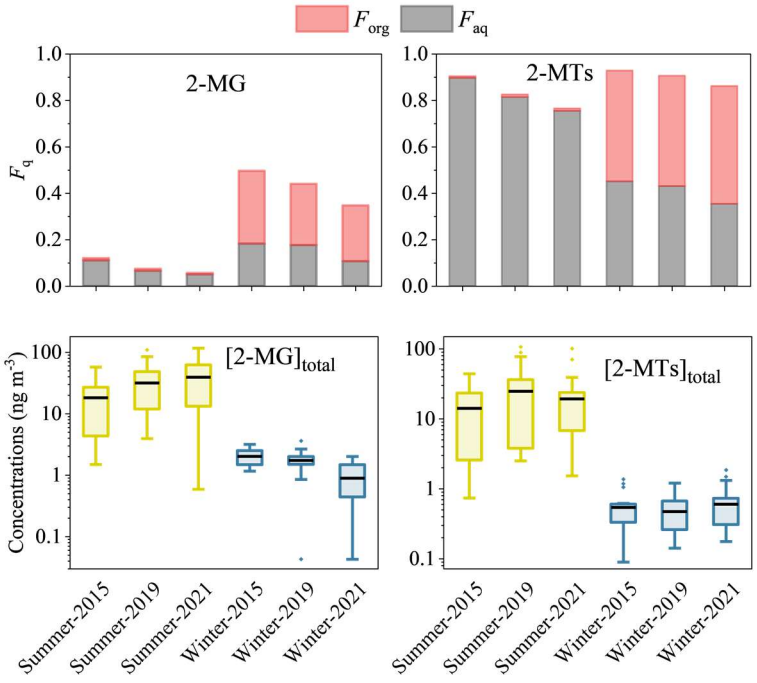

Figure S4. (a, b) Particle-phase fractions of 2-MG and 2-MTs estimated using an organic absorptive equilibrium partitioning model (F_{org}) and Henry's Law (F_{aq}); (c, d) Gas-plus-particle concentrations of 2-MG and 2-MTs derived using their estimated F_p values during the observation period.

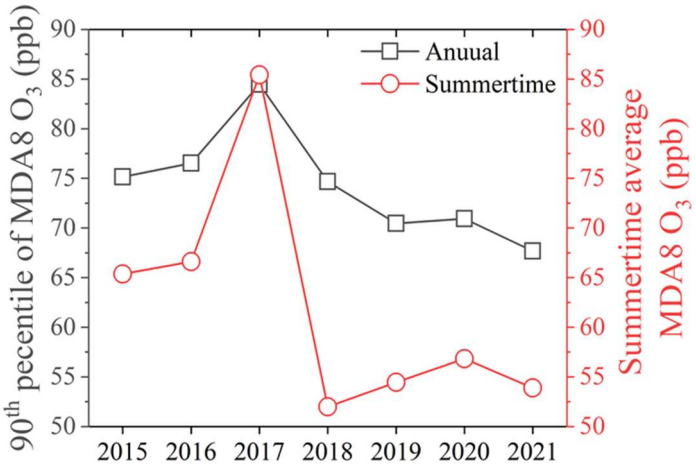

Figure S5. Annual 90th percentile of the maximum daily 8-h average (MDA8) O_3 concentrations in the region of Shanghai and summertime (10^{th} June to 10^{th} August) average MDA8 O_3values at the observation site from 2015 to 2021.

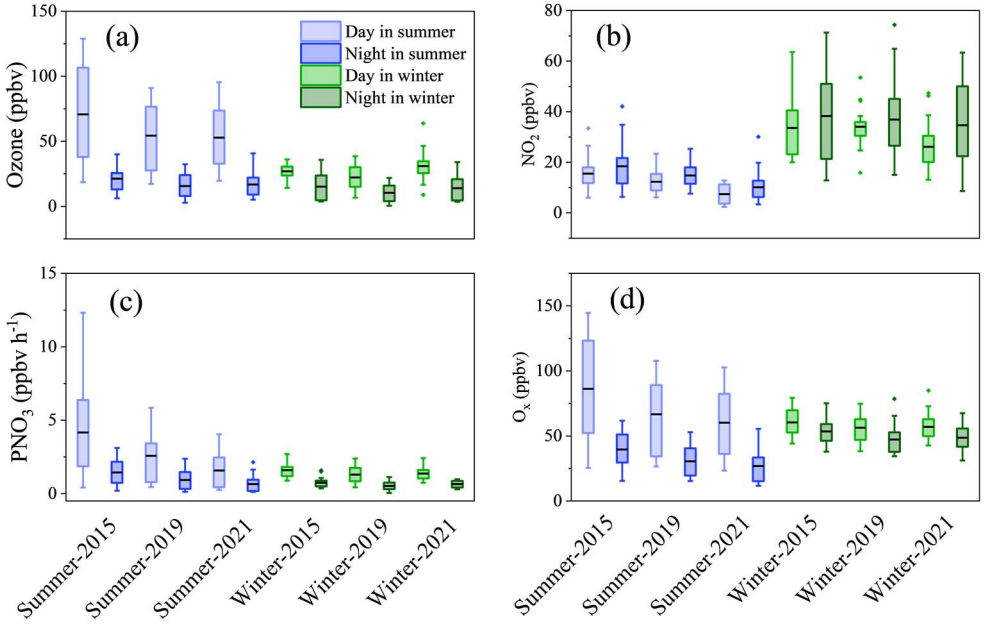

Figure S6. Box plots of concentrations of (a) ozone, (b) NO_2, (c) nitrate radical production rate (PNO_3), and (d) O_x in Shanghai. Blue and green boxes represent summer and winter respectively.

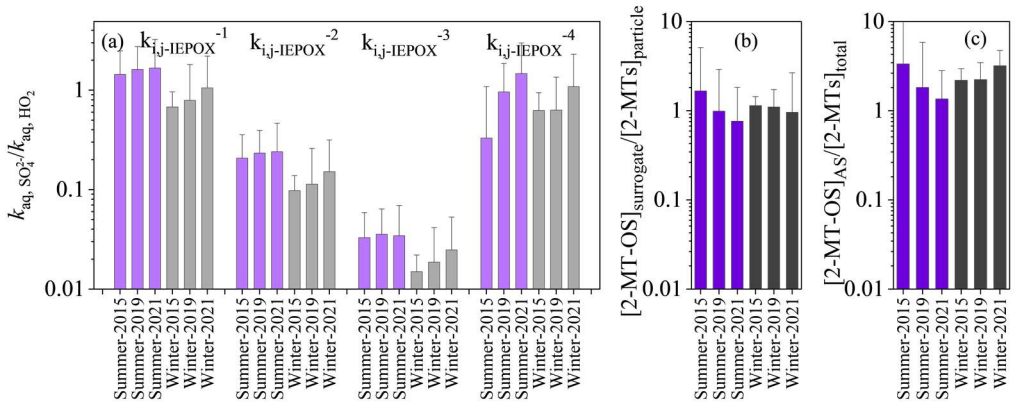

Figure S7. (a) Acid-catalyzed ring-opening reaction rates of IEPOX with sulfate vs. water ($k_{aq,\ SO_4^{2-}}/k_{aq,\ H_2O}$) calculated by different reaction rate values for specific nucleophiles list in Table S2, (b) measured ratios of particulate 2-MT-OS (quantified by the surrogate standard) to 2-MTs, and (c) measured ratios of gas-plus-particle-phase concentrations of 2-MT-OS (accounting for the uncertainties in the quantification using the surrogate standard) to 2-MTs.

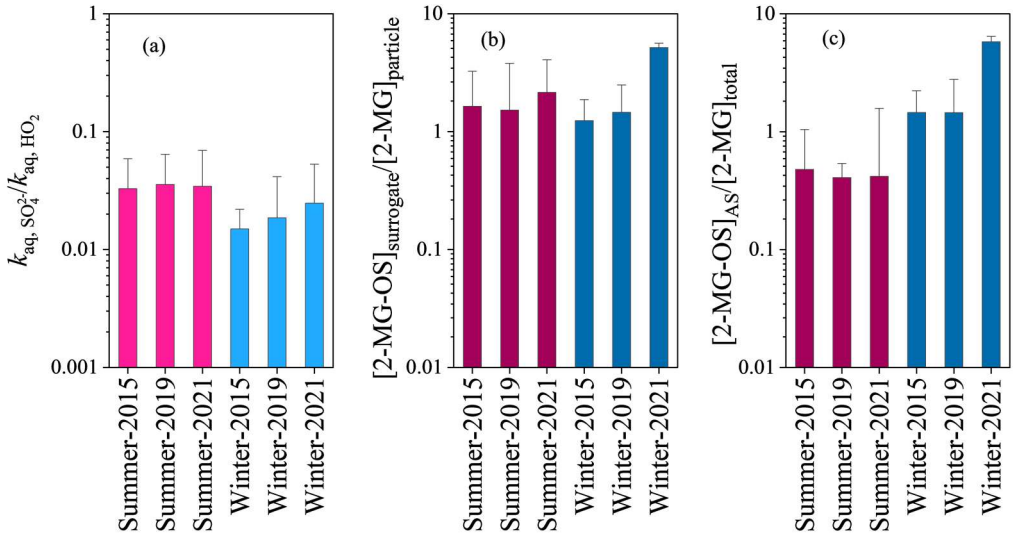

Figure S8. Comparisons between (a) estimated ratios of aqueous-phase reaction rates of HMML/MAE with sulfate to water and (b) measured ratios of particulate 2-MG-OS (quantified by the surrogate standard) to 2-MG and (c) measured ratios of gas-plus-particle-phase concentrations of 2-MG-OS (accounting for the uncertainties in the quantification using the surrogate standard) to 2-MG.

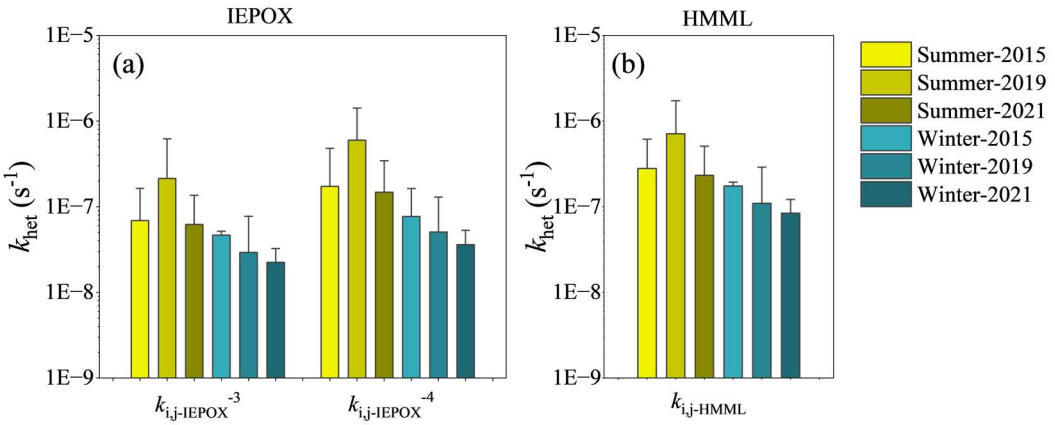

Figure S9. Values of k_{het} estimated by excluding the third-order reaction of the epoxide intermediate with bisulfate for (a) IEPOX and (b) HMML/MAE.

References

Brock, C. A., Wagner, N. L., Anderson, B. E., Attwood, A. R., Beyersdorf, A., Campuzano-Jost, P., Carlton, A. G., Day, D. A., Diskin, G. S., Gordon, T. D., Jimenez, J. L., Lack, D. A., Liao, J., Markovic, M. Z., Middlebrook, A. M., Ng, N. L., Perring, A. E., Richardson, M. S., Schwarz, J. P., Washenfelder, R. A., Welti, A., Xu, L., Ziemba, L. D., and Murphy, D. M.: Aerosol optical properties in the southeastern United States in summer - Part 1: Hygroscopic growth, Atmos. Chem. Phys., 16, 4987-5007, 10.5194/acp-16-4987-2016, 2016.

He, X., Wang, Q., Huang, X. H. H., Huang, D. D., Zhou, M., Qiao, L., Zhu, S., Ma, Y.-g., Wang, H.-l., Li, L., Huang, C., Xu, W., Worsnop, D. R., Goldstein, A. H., and Yu, J. Z.: Hourly measurements of organic molecular markers in urban Shanghai, China: Observation of enhanced formation of secondary organic aerosol during particulate matter episodic periods, Atmos. Environ, 240, 10.1016/j.atmosenv.2020.117807, 2020.

Huang, X.-F., Xue, L., Tian, X.-D., Shao, W.-W., Sun, T.-L., Gong, Z.-H., Ju, W.-W., Jiang, B., Hu, M., and He, L.-Y.: Highly time-resolved carbonaceous aerosol characterization in Yangtze River Delta of China: Composition, mixing state and secondary formation, Atmos. Environ, 64, 200-207, 10.1016/j.atmosenv.2012.09.059, 2013.

Liu, Y., Zhu, W., Wang, Y., Li, T., Tao, S., Qiao, L., Chen, J., Su, M., Shen, Q., and Lou, S.: Characterization of atmospheric submicron particles at an urban site in Shanghai in autumn using a high-resolution aerosol mass spectrometer, Acta Scientiae Circumstantiae, 38, 2746-2756, 2018.

Nguyen, T. B., Bates, K. H., Crounse, J. D., Schwantes, R. H., Zhang, X., Kjaergaard, H. G., Surratt, J. D., Lin, P., Laskin, A., Seinfeld, J. H., and Wennberg, P. O.: Mechanism of the hydroxyl radical oxidation of methacryloyl peroxynitrate (MPAN) and its pathway toward secondary organic aerosol formation in the atmosphere, Phys. Chem. Chem. Phys., 17, 17914-17926, 10.1039/c5cp02001h, 2015.

O'Meara, S., Booth, A. M., Barley, M. H., Topping, D., and McFiggans, G.: An assessment of vapour pressure estimation methods, Phys. Chem. Chem. Phys., 16, 19453-19469, 10.1039/c4cp00857j, 2014.

Pankow and James, F.: An absorption model of gas/particle partitioning of organic compounds in the atmosphere, Atmos. Environ, 28, 185-188, 1994.

Petters, M. D. and Kreidenweis, S. M.: A single parameter representation of hygroscopic growth and cloud condensation nucleus activity, Atmos. Chem. Phys., 7, 1961-1971, 10.5194/acp-7-1961-2007, 2007.

Pye, H. O. T., Pinder, R. W., Piletic, I. R., Xie, Y., Capps, S. L., Lin, Y.-H., Surratt, J. D., Zhang, Z., Gold, A., Luecken, D. J., Hutzell, W. T., Jaoui, M., Offenberg, J. H., Kleindienst, T. E., Lewandowski, M., and Edney, E. O.: Epoxide Pathways Improve Model Predictions of Isoprene Markers and Reveal Key Role of Acidity in Aerosol Formation, Environ Sci Technol, 47, 11056-11064, 10.1021/es402106h, 2013.

Pye, H. O. T., Murphy, B. N., Xu, L., Ng, N. L., Carlton, A. G., Guo, H., Weber, R., Vasilakos, P., Appel, K. W., Budisulistiorini, S. H., Surratt, J. D., Nenes, A., Hu, W., Jimenez, J. L., Isaacman-VanWertz, G., Misztal, P. K., and Goldstein, A. H.: On the implications of aerosol liquid water and phase separation for organic aerosol mass, Atmos. Chem. Phys., 17, 343-369, 10.5194/acp-17-343-2017, 2017.

Rasool, Q. Z., Shrivastava, M., Octaviani, M., Zhao, B., Gaudet, B., and Liu, Y.: Modeling Volatility-Based Aerosol Phase State Predictions in the Amazon Rainforest, ACS Earth Space Chem, 5, 2910-2924, 10.1021/acsearthspacechem.1c00255, 2021.

Wang, Y., Zhao, Y., Wang, Y., Yu, J.-Z., Shao, J., Liu, P., Zhu, W., Cheng, Z., Li, Z., Yan, N., and Xiao, H.: Organosulfates in atmospheric aerosols in Shanghai, China: seasonal and

interannual variability, origin, and formation mechanisms, Atmos. Chem. Phys., 21, 2959-2980, 10.5194/acp-21-2959-2021, 2021.

Wania, F., Lei, Y. D., Wang, C., Abbatt, J. P. D., and Goss, K. U.: Using the chemical equilibrium partitioning space to explore factors influencing the phase distribution of compounds involved in secondary organic aerosol formation, Atmos. Chem. Phys., 15, 3395-3412, 10.5194/acp-15-3395-2015, 2015.

Yang, T., Xu, Y., Ye, Q., Ma, Y. J., Wang, Y. C., Yu, J. Z., Duan, Y. S., Li, C. X., Xiao, H. W., Li, Z. Y., Zhao, Y., and Xiao, H. Y.: Spatial and diurnal variations of aerosol organosulfates in summertime Shanghai, China: potential influence of photochemical processes and anthropogenic sulfate pollution, Atmos. Chem. Phys., 23, 13433-13450, 10.5194/acp-23-13433-2023, 2023.

Yee, L. D., Isaacman-Vanwertz, G., Wernis, R. A., Kreisberg, N. M., and Goldstein, A. H.: Natural and anthropogenically-influenced isoprene oxidation in the Southeastern U.S.A. and central Amazon, Environ Sci Technol, 54, 2020.

Zhang, J., Liu, J., Ding, X., He, X., Zhang, T., Zheng, M., Choi, M., Isaacman-VanWertz, G., Yee, L., Zhang, H., Misztal, P., Goldstein, A. H., Guenther, A. B., Budisulistiorini, S. H., Surratt, J. D., Stone, E. A., Shrivastava, M., Wu, D., Yu, J. Z., and Ying, Q.: New formation and fate of Isoprene SOA markers revealed by field data-constrained modeling, npj Clim. Atmos. Sci., 6, 69, 10.1038/s41612-023-00394-3, 2023.